

pubs.acs.org/biochemistry Article

Determinants of Multiheme Cytochrome Extracellular Electron Transfer Uncovered by Systematic Peptide Insertion

Ian J. Campbell, Joshua T. Atkinson, Matthew D. Carpenter, Dru Myerscough, Lin Su, Caroline M. Ajo-Franklin, and Jonathan J. Silberg*



Cite This: https://doi.org/10.1021/acs.biochem.2c00148



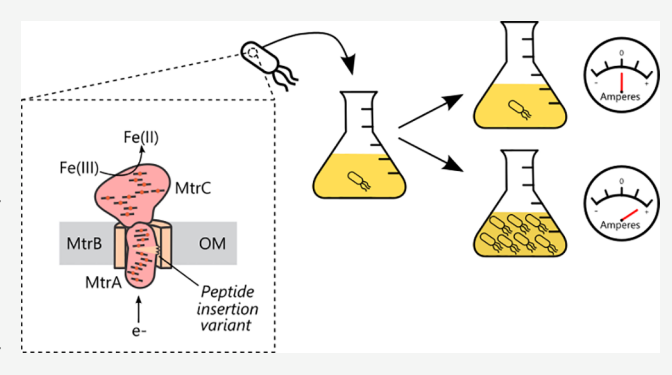
ACCESS I

III Metrics & More

Article Recommendations

SI Supporting Information

ABSTRACT: The multiheme cytochrome MtrA enables microbial respiration by transferring electrons across the outer membrane to extracellular electron acceptors. While structural studies have identified residues that mediate the binding of MtrA to hemes and to other cytochromes that facilitate extracellular electron transfer (EET), the relative importance of these interactions for EET is not known. To better understand EET, we evaluated how insertion of an octapeptide across all MtrA backbone locations affects Shewanella oneidensis MR-1 respiration on Fe(III). The EET efficiency was found to be inversely correlated with the proximity of the insertion to the heme prosthetic groups. Mutants with decreased EET efficiencies also arose from insertions in a subset of the regions that make residue—residue contacts with the porin



MtrB, while all sites contacting the extracellular cytochrome MtrC presented high peptide insertion tolerance. MtrA variants having peptide insertions within the CXXCH motifs that coordinate heme cofactors retained some ability to support respiration on Fe(III), although these variants presented significantly decreased EET efficiencies. Furthermore, the fitness of cells expressing different MtrA variants under Fe(III) respiration conditions correlated with anode reduction. The peptide insertion profile, which represents the first comprehensive sequence–structure–function map for a multiheme cytochrome, implicates MtrA as a strategic protein engineering target for the regulation of EET.

ultiheme cytochrome electron transfer proteins have evolved to support the exchange of electrons between cells and the extracellular environment. 1,2 By binding a series of adjacent cofactors that span tertiary structures, these proteins enable electron transport across the insulating membrane and across micrometer-scale distances by insulating the heme prosthetic groups from the solvent.³⁻⁶ This highefficiency electron transport enables diverse microorganisms to respire on extracellular metals, minerals, and materials.^{2,7–9} The Gram-negative bacterium Shewanella oneidensis has evolved a cytochrome-based pathway, designated the metalreducing pathway (Mtr), to support extracellular electron transfer (EET). 10,111 This pathway allows microbes to respire on Fe(III), Mn(III), and Mn(IV). Additionally, the Mtr pathway can reduce extracellular minerals, like hematite or ferrihydrite, as well as synthetic nanoparticles and electrodes.^{7,12-17}

Among the different EET systems that have been reported, the Mtr pathway of *S. oneidensis* has been studied most intensively. ^{18–20} In this pathway, multiheme cytochromes housed within porins transfer reducing equivalents generated by catabolic processes through the outer membrane. ^{21–23} While *S. oneidensis* encodes multiple cytochrome—porin complexes, the complex with the highest flux of electrons is

MtrCAB (UniProt entries Q8EG34, Q8EG35, and Q8CVD4).²² MtrC is required for appreciable reduction of ferric citrate, iron oxides, and flavins.^{15,22} The loss of MtrC leads to a large loss of current supplied to an electrode and a decreased level of reduction of synthetic materials, including UO₂ and Pd nanoparticles.^{15–17} Similarly, loss of MtrA weakens the ability of *S. oneidensis* to reduce ferric citrate, iron oxide, and flavins, an effect that is amplified when coupled with knockouts of MtrA paralogs.²²

Structural studies have provided atomistic insight into molecular interactions within the MtrCAB complex. ^{20,24} The decaheme cytochrome MtrA resides within MtrB, a porin that spans the extracellular membrane. The decaheme MtrC binds to the extracellular face of the MtrAB complex and supports electron transfer to exogenous electron acceptors by offering a large surface area with multiple surface-exposed hemes. ^{20,22}

Received: March 15, 2022 Revised: June 2, 2022



Spectroscopic and simulation studies have found that electrons can pass between adjacent heme prosthetic groups within the MtrCAB complex at nanosecond rates and suggested that these rapid transfers are facilitated by cysteine linkages positioned between those tetrapyrroles. In MtrA, heme A10 is thought to mediate interprotein electron transfer to heme C5 of MtrC. Electron transfer between these hemes, which have an edge—edge distance of 8 Å, is thought to be rate limiting for EET through the MtrCAB complex. While these studies have revealed a complex network of molecular interactions within the Mtr complex, including protein—cofactor and protein—protein interactions, we cannot yet anticipate how changes to the primary structure of MtrCAB affect EET.

One way to probe the importance of native residues in mediating protein—cofactor and protein—protein interactions is to evaluate the effects of mutations on cellular function. ^{25–27} In cases in which a high-throughput selection is available, large numbers of mutations can be evaluated in parallel using laboratory evolution. ^{26–28} With this approach, a library of genes encoding mutant proteins is created, and the library is subjected to next generation sequencing before and after selection for biomolecules with parent-like functions. ²⁹ The changes in the abundance of each mutant are then used to calculate the ratio of sequence counts before and after selection, which can be used to estimate the relative activities of mutant proteins. This approach has been applied to diverse proteins that function in cellular catalysis. ^{30–33} However, it has not yet been applied to multiheme cytochromes that mediate EET.

To study sequence—structure—EET relationships in MtrA, we created a library of variants with the peptide SGRPGSLS inserted at every backbone position and selected this library for variants that support EET. We generated insertional mutations rather than amino acid substitutions because they have the potential to create a higher level of structural disruption at each native site due to the need to accommodate a large change in primary structure. By quantifying variant abundances in our library before and after selection, we identify regions that present varying EET efficiencies following peptide insertion. We show that the sequence enrichments observed in our selection correlate with EET of individual variants and evaluate how peptide insertion in partner-binding regions and CXXCH motifs affect EET to Fe(III), nanoparticles, and electrodes.

METHODS

Strains. Escherichia coli XL1-Blue was from Agilent, and dam-/dcm- E. coli was obtained from New England Biolabs. S. oneidensis JG665 ($So-\Delta mtrA$) was a kind gift from J. Gralnick, ²² while S. oneidensis MR-1 was from the American Type Culture Collection.

Plasmid Construction. Plasmids are listed in Table S1. Endogenous genes were synthesized as G-blocks by Integrated DNA Technologies, and plasmids were constructed by using Q5 High-Fidelity DNA polymerase (New England Biolabs) to produce amplicons and ligating amplicons to PCR-amplified vectors using Golden Gate DNA assembly.³⁴ The broad-range RSF1010 backbone was used for all plasmids and was generously provided by S. Bhakta.³⁵ All plasmid sequences were verified with Sanger sequencing.

Library Generation. The MtrA protein (UniProt entry Q8EG35) was used for library creation. Oligonucleotides encoding MtrA gene fragments with insertions encoding SGRPGSLS were designed using the SPINE algorithm.²⁸

Gene tiles synthesized as an oligo pool by Twist Bioscience were PCR amplified using Q5 High-Fidelity DNA polymerase and cloned into vector RSF1010 using Golden Gate cloning. Plasmid ensembles were transformed into E. coli XL1-Blue and plated onto lysogeny broth (LB) agar plates containing 50 μ g/ mL kanamycin. The transformations for each tile yielded >2500 colony-forming units (CFU). Assuming sampling with replacement, this colony count indicates that >99% of our variants were sampled at this step.³⁶ Colonies were harvested from plates and pooled, and plasmid DNA was purified using a Qiagen Miniprep kit. The distribution of insertion sites was evaluated using Amplicon-EZ sequencing (Genewiz). The library was then transformed into dam-/dcm- E. coli (New England Biolabs), and sufficient colony counts were obtained to sample >99% of our variants. The demethylated insertion library was transformed into S. oneidensis So-ΔmtrA using electroporation and plated on LB agar plates containing 50 μ g/ mL kanamycin. The naive library harvested from these plates was stored as a glycerol stock.

Growth Complementation. *So-\Delta mtrA* cells transformed with plasmids expressing mtrA or empty vector were grown alongside S. oneidensis MR-1 transformed with a vector bearing mtrA overnight at 30 °C and 250 rpm in Shewanella Basal Medium (SBM) containing 8.6 mM NH₄Cl, 1.3 mM K₂HPO₄, 1.65 mM KH₂PO₄, 475 μ M MgSO₄·7H₂O, 1.7 mM (NH₄)₂SO₄, 7.5 mg/L nitrilotriacetic acid, 0.5 mg/L MnCl₂· 4H₂O, 1.5 mg/L FeSO₄·7H₂O, 0.85 mg/L CoCl₂·6H₂O, 0.5 mg/L ZnCl₂, 0.2 mg/L CuSO₄·5H₂O, 0.025 mg/L AlK- $(SO4)_2 \cdot 12H_2O_1 \cdot 0.025 \text{ mg/L } H_3BO_3, 0.45 \text{ mg/L } Na_2MoO_4, 0.6$ mg/L anhydrous NiCl₂, 0.1 mg/L NaWO₄·2H₂O, 0.5 mg/L Na₂SeO₄, 0.01 mg/L biotin, 0.01 mg/L folic acid, 0.1 mg/L pyridoxine HCl, 0.025 mg/L thiamine, 0.025 mg/L nicotinic acid, 0.025 mg/L pantothenic acid, 0.5 µg/L cyanocobalamin, 0.025 mg/L p-aminobenzoic acid, 0.025 mg/L α -lipoic acid, 100 mM HEPES (pH 7.2), 0.05% (w/v) casamino acids, 20 mM lactate, and 50 μ g/mL kanamycin.³⁷ Overnight cultures were diluted 1:100 in fresh SBM supplemented with either 30 mM ferric citrate or 30 mM fumarate and transferred to a 96well plate. The plate was incubated in a N2 atmospheric chamber at 30 °C and shaken at 500 rpm. Optical density measurements at 600 nm (OD₆₀₀) were taken after 48 h using a Tecan Spark plate reader.

Library Selections. The glycerol stock of the naïve library was used to inoculate SBM medium that was grown for 18 h aerobically at 30 °C while being shaken at 250 rpm. To evaluate the sequence diversity in the naïve library, three separate overnight cultures were harvested and subjected to deep sequencing (Genewiz). An aliquot of each culture was also diluted into fresh SBM medium to an OD_{600} of 0.1 and used to inoculate sealed bottles containing either SBM supplemented with 30 mM fumarate (n = 3) or SBM supplemented with 30 mM ferric citrate (n = 3). This growth medium was sparged for 30 min with N_2 prior to inoculation and filtered to remove all undissolved ferric citrate. After being incubated for 24 h, cells were harvested, and samples were sent for deep sequencing.

Sequence Analysis. Table S2 provides the relative abundances of each variant observed in the three different naive, unselected, and selected libraries. Variants were numbered using the native residue that immediately follows the peptide insertion; e.g., IV-261 represents the variant having a peptide inserted before Pro261. Insertion sites identified from deep sequencing were processed using the DIP-seq

algorithm.³⁸ Two sequence enrichments were calculated for each variant: enrichment after the selective growth in ferric citrate relative to the naive condition (ε_s) and enrichment after nonselective growth in fumarate relative to the naive condition $(\varepsilon_{\rm n})$. Enrichments were calculated by dividing the frequency (f_i) of each variant observed under ferric citrate (f_s) or fumarate (f_n) conditions by the frequency of each variant in the naive library. The frequencies of the naive and nonselective insertion libraries were then fit to a linear regression using NumPy.³⁹ A z score for ε_s values was generated by subtracting the mean of the ε_n distribution (μ_n) and normalizing by the standard deviation of the $\varepsilon_{\rm n}$ distribution ($\sigma_{\rm n}$). Values of zscored ε_s were overlaid onto the structure of MtrA from Shewanella baltica [Protein Data Bank (PDB) entry 6r2q]²⁰ and visualized using PyMol (Schrodinger, LLC, 2010, The PyMOL Molecular Graphics System, version 2.5).

MoO₃ Nanoparticle Assay. Cultures grown for 16 h in LB containing 50 µg/mL kanamycin were pelleted using centrifugation (4000g) for 10 min at room temperature, washed with an M9 medium containing sodium phosphate dibasic (6.8 g/L), sodium phosphate monobasic (3 g/L), sodium chloride (0.5 g/L), 2% glucose, ammonium chloride (1 g/L), and 20 mM lactate, and resuspended to an OD_{600} of 1. Resuspended cultures were mixed at a 1:1 ratio with 10 mg/ mL molybdenum trioxide (MoO₃) nanoparticles (Sigma-Aldrich) and incubated for 15 min in a 96-well plate at room temperature in a 5% $H_2/10\%$ $CO_2/85\%$ N_2 atmosphere. Cultures were scanned using a CanoScan LiDE 220 instrument, and the blueness of wells was determined using ImageI with the ReadPlate3 plugin. 40 The experiment comparing MoO₃ and WO₃ was conducted in the same manner except that precultures were grown to an OD₆₀₀ of 5 and incubated for 10 min; for these measurements, we compared only S. oneidensis MR-1 EET. WO₃ and MoO₃ nanoparticles (<100 nm) were from Sigma.

Enhanced Chemiluminescence Staining. Cultures grown for 16 h in LB containing kanamycin (50 μ g/mL) were pelleted (4000g) for 10 min at room temperature and washed with M9 medium as in the MoO3 assay. Cultures having the same optical density were mixed in a 1:1 ratio with a gel loading solution containing mercaptoethanol (0.71 M) and 1× LDS Loading Dye Mix (NuPage), and this mixture was incubated for 15 min. Samples were then loaded onto a 12% Bis-Tris gel (Invitrogen) and run for 20 min at 200 mV with a Precision Plus Protein Dual Color Standards ladder. Protein samples were transferred to blotting paper using a Trans-Blot Turbo Transfer Pack (Bio-Rad) and a Trans-Blot Turbo (Bio-Rad) using the "1 mini gel" setting. Cytochromes were visualized using Clarity Western ECL Substrate (Bio-Rad) and then imaged for both visible and chemiluminescent signals using a FluorChem E imager (ProteinSimple). Chemiluminescent images were overlaid on visible images to compare protein standards and chemiluminescent cytochromes.

Chronoamperometry. Each biological replicate was derived from a different colony picked from an LB-agar plate (with 50 μ g/mL kanamycin) streaked with cells from a glycerol stock. Picked colonies were used to inoculate 5 mL cultures of LB with 50 μ g/mL kanamycin that were grown for 16–20 h at 30 °C, while being shaken at 250 rpm. These cultures were then used to inoculate 50 mL LB cultures (with 50 μ g/mL kanamycin) in 250 mL flasks to a standardized OD₆₀₀ of 0.01. The resulting 50 mL cultures were grown for 20 h at 30 °C, while being shaken at 250 rpm. Cells were pelleted via

centrifugation, and the LB was removed. The cell pellets were washed twice with 25 mL of M9 minimal salts (BD). The anodic chambers of dual-chamber bioelectrochemical reactors were inoculated to a standardized OD_{600} of 0.5 using 3 mL of cells resuspended in M9 minimal salts. The anodic chamber contained a carbon felt working electrode (geometric surface area of 0.0022 m², Alfa Aesar) suspended from a 1 mm diameter titanium wire, a Ag/AgCl (3 M KCl, CHI111, CH Instruments) reference electrode, and 117 mL of M9 minimal salts with 30 mM D,L-lactate (Sigma). This chamber was separated by a cation exchange membrane (CMI-7000, Membranes International) from a cathodic chamber containing 115 mL of M9 minimal salts and a 1 mm diameter titanium wire counter electrode. All electrodes were connected to a BioLogic VMP-300 potentiostat. The anodic chamber was continuously stirred with a stir bar at 300 rpm, temperaturecontrolled at 30 °C, and sparged with N₂ gas to maintain anaerobic conditions. The working electrode was poised at 0.2 V versus Ag/AgCl, and the average current was recorded every

Structural Analysis and Modeling. The crystal structure of the S. baltica MtrCAB complex (PDB entry 6R2Q) was used for analysis.²⁰ Unresolved loops near the N-terminus of MtrA were reconstructed using Rosetta's loopmodeler application on default settings using the beta nov16-genpot force field, 41 with MtrB, MtrC, and the heme prosthetic groups included. The lowest scoring of 500 structures from Rosetta was used for all further analysis unless otherwise specified. The axial position of each residue was calculated as the distance from the $C\alpha$ atom of the residue to the x-z plane normal to the long dimension of MtrA and centered at the $C\alpha$ atom of lysine 62, the most intracellular residue resolved in the crystal structure. The radial position of each residue was calculated as the distance from the $C\alpha$ atom of the residue to the center axis defined by the average x and z coordinates of the iron atoms of all hemes in MtrA. To determine the per-residue contact density, shortrange contacts were identified between residues with a cutoff of 8 Å between $C\alpha$ atoms, and both short- and long-range contacts were identified with a cutoff of 14 Å, which is commonly used. 42-44 Contacts were counted separately for residues within MtrA as well as between MtrA and MtrB and between MtrA and MtrC. $C\alpha$ B factors were obtained from the crystal structure for each residue in MtrA using the Biopython Bio.PDB package^{45,46} and averaged for the residue preceding and the residue following each insertion site. Per-residue stiffness estimates were obtained from a $C\alpha$ anisotropic network model of the entire MtrCAB complex (without hemes) using the ProDy suite, 47,48 based on previously described protocols.44,49

Statistics. All error bars represent ± 1 standard deviation calculated from three or more biological replicates. Independent, two-tailed t tests were used to compare differences among all relevant samples with an α of 0.05. All correlations shown are Spearman correlations calculated with Pandas. ⁵⁰

RESULTS

MtrA Library Design and Selection. In a prior study, a *S. oneidensis* mutant was created that lacks MtrA, three MtrA paralogs (MtrD, DmsE, and SO4360), and a periplasmic electron carrier (CctA).²² The ability of this strain, designated *So-ΔmtrA* herein, to reduce ferric citrate is severely diminished. Because *S. oneidensis* can respire on extracellular sources of iron using the Mtr pathway, we reasoned that *So-ΔmtrA* growth

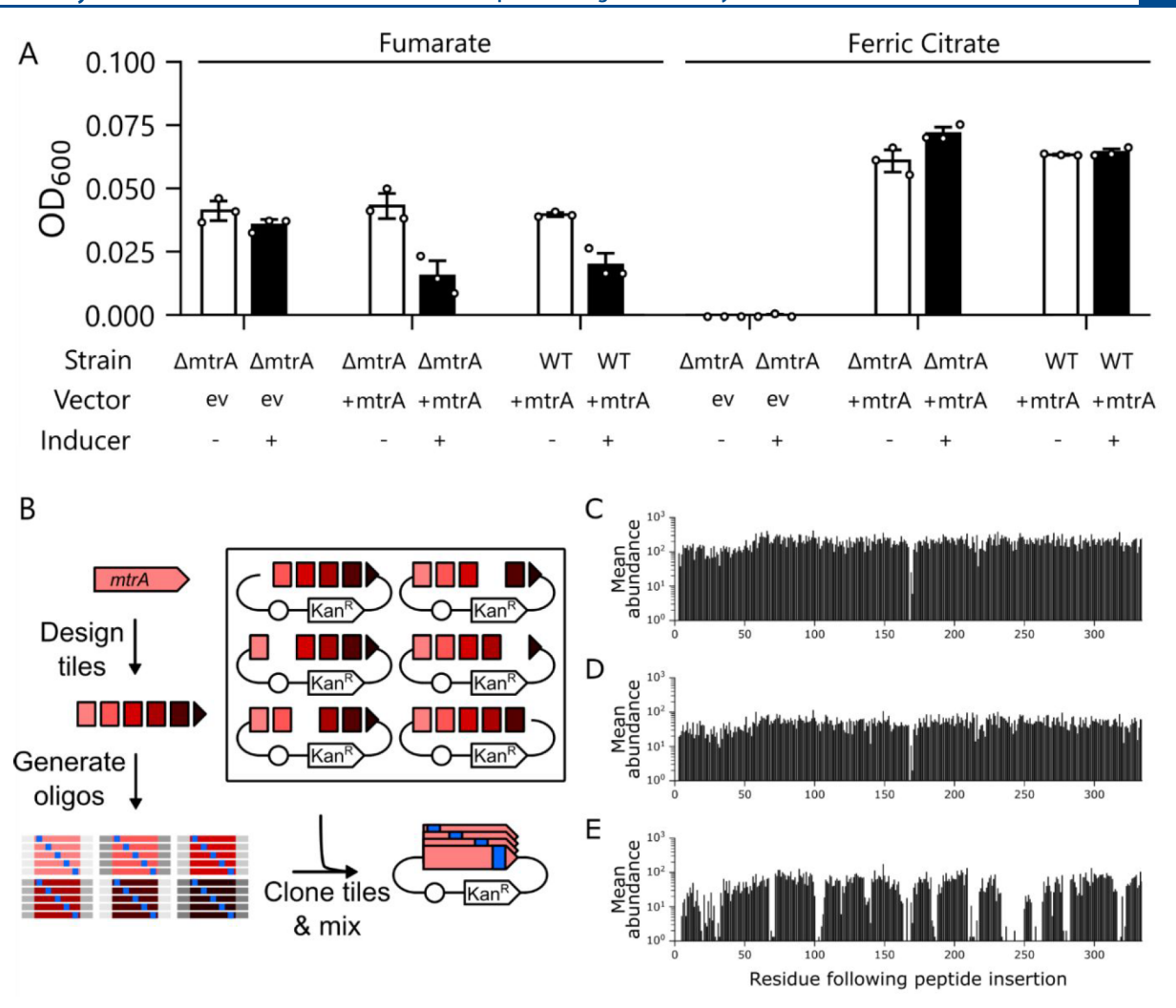


Figure 1. Using laboratory evolution to evaluate MtrA tolerance to peptide insertion. (A) So- Δ mtrA requires MtrA for growth complementation on Fe(III). So- Δ mtrA strains transformed with an empty vector (ev) or a plasmid expressing MtrA (+mtrA) were grown for 48 h at 30 °C in an anaerobic atmosphere using either fumarate or ferric citrate as the sole electron acceptor in the presence (black) or absence (white) of an inducer. As a control, we also evaluated S. oneidensis MR-1 (WT) expressing MtrA. Error bars represent the standard deviation calculated from three experiments. With ferric citrate, cells expressing MtrA grew to a significantly higher density than cells containing an empty vector (P < 0.01; two-tailed t test), and the growth of these cells was not significantly different from that of S. oneidensis MR-1 expressing MtrA (P > 0.1; two-tailed t test). (B) Using the SPINE algorithm, the MtrA sequence was fragmented into six tiles in silico, each having a length (<300 bp) that could be commercially synthesized using pooled oligonucleotide synthesis. The algorithm designed oligonucleotides encoding every unique eight-codon insertion within the tile, and it added unique barcodes to the ends of each tile ensemble to allow for selective amplification. PCR-amplified tiles were cloned into vector backbones complementary to each tile using Golden Gate cloning to generate an insertion library. Deep sequencing was used to determine the average frequency (f_i) of insertion sites across the MtrA library in (C) the naïve preculture, (D) cells grown anaerobically with fumarate, and (E) cells grown anaerobically with ferric citrate. For each condition, we show the average of three separate experiments.

could be complemented by MtrA expression under anaerobic conditions when ferric citrate was provided as a terminal electron acceptor. 11,22 To test this idea, we created plasmids that express MtrA using the $P_{LtetO-1}$ promoter, transformed So- $\Delta mtrA$ with these plasmids, and evaluated growth under selective (with ferric citrate) and nonselective (with fumarate) growth conditions. Under selective conditions, growth was not observed with $So-\Delta mtrA$ harboring an empty vector (Figure 1A). In contrast, robust growth was observed with So- $\Delta mtrA$ expressing MtrA, which was similar to that observed with wildtype S. oneidensis MR-1 expressing MtrA. The growth complementation observed with So-AmtrA expressing MtrA did not require an inducer, indicating that our expression system is leaky. All strains grew to a similar extent under nonselective conditions in the absence of an inducer when provided with fumarate as an electron acceptor, which is

directly reduced by the periplasmic cytochrome FccA without the need for EET through MtrA. When an inducer was included in the cultures containing fumarate, the level of growth was decreased, suggesting that MtrA expression causes a fitness burden under this growth condition. Taken together, these findings suggest that $So-\Delta mtrA$ can be used to mine combinatorial libraries of MtrA variants for multiheme cytochromes that support EET.

To design a library of vectors that express MtrA variants with a peptide inserted at different native sites, we used a previously described algorithm called SPINE. We synthesized oligonucleotides that encode MtrA variants with a 24 bp insertion, encoding SGRPGSLS, inserted between every codon. With SPINE, this peptide was generated because a unique restriction site was inserted between each pair of adjacent codons in the MtrA gene. This vector library was built

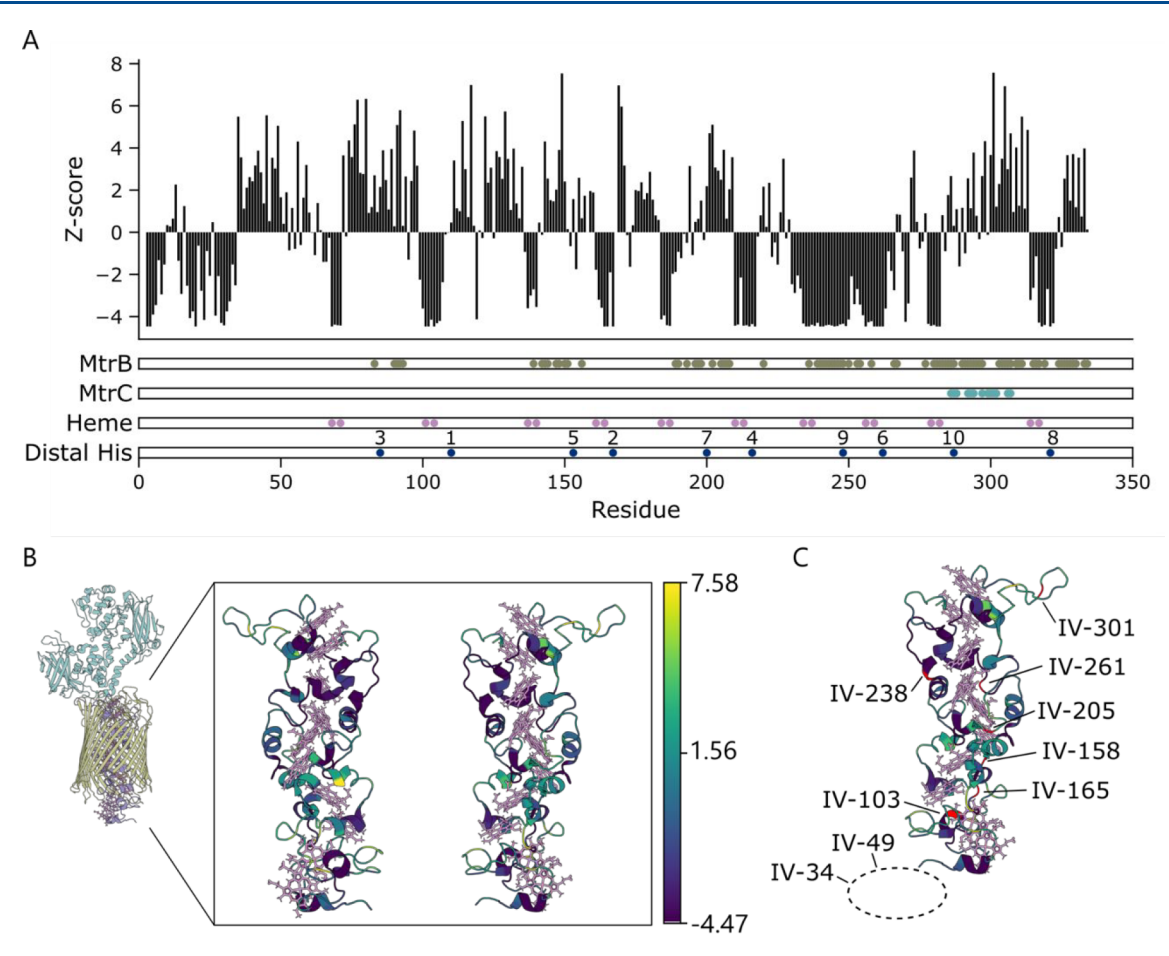


Figure 2. Effect of growth selection on MtrA mutant abundances. (A) Enrichment values for the nonselected furnarate (${}^n\varepsilon_i$) and selected ferric citrate (${}^s\varepsilon_i$) cultures were calculated by dividing the frequencies observed for each mutant under the different growth conditions by the frequencies present under the naïve aerobic condition. The distribution of z-scored selected enrichments was then calculated from the selected enrichments (${}^s\varepsilon_i$) normalized by the nonselective enrichment distribution (${}^n\varepsilon$). MtrA residues are highlighted that contact MtrB (dark green), contact MtrC (teal), represent the cysteines in the CXXCH motifs (pink), and serve as the distal histidine ligands (dark blue). The hemes ligated by each distal histidine are also noted. A distance cutoff of 8 Å was used to define the contacts. (B) The MtrA structure is color-coded using the z scores observed in the mutational profile, and (C) the insertion variants that were further characterized (red) are noted on the structure. A sequence alignment of MtrA from S. baltica and S. oneidensis MR-1 (Figure S13) was used to relate our selection data to published structural data.

using a tile-based cloning approach (Figure 1B). With this approach, the full length MtrA gene was broken into six tiles, and ensembles of synthetic DNA (~230 bp) were cloned in parallel to replace the native sequence at different locations. To achieve a high transformation efficiency of So- $\Delta mtrA$ critical to library sampling, we demethylated the plasmid library by first transforming it into E. coli lacking the Dam and Dcm methylation machinery. 52,53 The demethylated library was then electroporated into So- $\Delta mtrA$. This protocol yielded a CFU count (~20000) that is predicted to sample >99% of all variants in the library. 36 So- $\Delta mtrA$ cells transformed with the library were harvested, pooled, and cultured aerobically in triplicate. Aliquots of each culture ($\sim 10^6$ CFU) were used to inoculate growth medium (100 mL) containing either ferric citrate or fumarate as the terminal electron acceptor, and these cultures were incubated under anaerobic conditions. Large cultures were used to ensure that cells would undergo a large number of doublings as they grew to stationary phase, thereby enabling the discovery of MtrA variants with a wide range of EET activities. All growth was performed in the absence of an inducer because $So-\Delta mtrA$ expressing MtrA grew to a similar extent on ferric citrate in the presence and absence of an inducer.

To examine the effect of growth complementation on MtrA mutant abundance, deep sequencing was used to quantify the relative abundance of each variant grown in (i) the naive aerobic So- $\Delta mtrA$ cultures used for inoculation, (ii) the nonselective anaerobic fumarate cultures, and (iii) the selective anaerobic ferric citrate cultures. We first evaluated how the sequence biases in the inoculum compared to libraries created using transposase-mediated insertion, 28,54-57 which can present large sequence biases in naïve libraries. Deep sequencing revealed that all of the variants were present in the naive library except the variant having the peptide inserted before Val168 (Figure 1C and Figure S1). The average abundance of each unique variant was 3 per 1000 sequence reads with a standard deviation of 1.2 per 1000 reads. The coefficient of variance for mutant abundance [CV = 0.37] (Figure S2a)] was much smaller than that observed in libraries created using transposases. 54-57 Sequencing revealed similar relative abundances of insertion variants in samples after anaerobic growth with fumarate (Figure 1D and Figure S3). The nonselective conditions yielded a CV (0.39) similar to that of the naïve library (Figure S2b). Additionally, the average abundance of each variant in the naive and nonselective conditions exhibited a linear correlation (Figure S4), with a

slope (0.93) and *y*-intercept (near 0) that are close to that expected (1 and 0, respectively) if growth on fumarate is nonselective to the variants in the library. This finding suggests that MtrA mutations do not have strong effects on $So\text{-}\Delta mtrA$ fitness when using fumarate as a terminal electron acceptor. Analysis of the MtrA sequence diversity in cells cultured on ferric citrate revealed more dramatic changes in the relative abundances of each variant (Figure 1E and Figure S5), with multiple variants being absent. Under selective conditions, a skewed distribution was observed with a CV of 0.82 (Figure S2c). These findings suggest that a subset of the peptide insertions alter EET mediated by MtrA.

To compare the effects of peptide insertion at different backbone locations on Mtr-mediated EET, we calculated the relative frequency of each variant (f_i) by quantifying the ratio of the reads for that variant (r_i) to the total sample reads (r_{total}) under the different growth conditions. To establish the enrichment of each variant under selective (ε_s) and nonselective (ε_n) conditions, we then calculated the ratio of f_i obtained under selective conditions (${}^{s}f_{i}$) to the naive condition $\binom{n}{i}$ and the ratio of f_i obtained under nonselective conditions $\binom{ns}{f_i}$ to the naive condition $\binom{nf_i}{z}$. z scores were then calculated for each variant by subtracting the mean ε_n for all variants from the $\varepsilon_{\rm s}$ values for the individual variants and normalizing the resulting values to the standard deviation of the ε_n values. The sequence enrichment varied across the primary structure. The most highly enriched sequences on ferric citrate had a z score of 7.57 (Figure 2A), while the most depleted sequences had zscores of -4.47; variants with the lowest z scores were not observed by deep sequencing following the ferric citrate selection. Mapping these z scores onto the S. baltica MtrA crystal structure reveals that regions of low and high peptide insertion tolerance are dispersed across the tertiary structure (Figure 2B). Also, the CXXCH motifs that become covalently attached to the 10 heme prosthetic groups have uniformly low z scores, while the axial histidine ligands outside of these motifs present a wider range of z scores. In summary, a comparison of the sequencing data from each growth condition identified MtrA variants that complement So- $\Delta mtrA$ to differing extents, implicating these variants as transferring electrons across the outer member with a range of efficiencies.

MtrA Mutant Enrichments Correlate with Respiration **on Ferric Citrate.** To understand how the z scores observed for different variants relate to EET mediated by specific MtrA mutants, we chose six variants to characterize individually. For these measurements, we chose peptide insertion variants (IV) with the full spectrum of z scores (Table 1, Figure 2C, and Figure S6). These variants sample MtrA regions that make a high density of contacts with MtrB (IV-158, IV-205, and IV-261) and MtrC (IV-301), as well as the structurally unresolved N-terminal region that extends into the periplasm (IV-34 and IV-49). Expression vectors for each variant were transformed into So- $\Delta mtrA$, and growth complementation was measured in anaerobic cultures containing ferric citrate as a terminal electron acceptor. As controls, we also evaluated cells transformed with an empty vector and a native MtrA expression vector. After 24 h (Figure 3A), all strains grew to a greater extent than the empty vector control with the exception of cells expressing IV-261. Additionally, cells expressing IV-301 grew to a significantly higher density than cells expressing native MtrA. A comparison of the z scores from the library analysis and OD_{600} from growth comple-

Table 1. MtrA Insertion Variants Targeted for Characterization^a

name	residue	z score	flanking sites	plasmid
IV-34	A34	-2.52	TPNAY-ASKWD	pIC014
IV-49	T49	5.05	EQVEA-TLDKK	pIC017
IV-103	C103	-4.14	LQCEA-CHGPL	pIC032
IV-158	V158	-0.003	HDNAD-VACAS	pIC015
IV-165	Q165	-4.47	CASCH-QVHVA	pIC036
IV-205	A205	2.49	HPLKW-AQMTC	pIC016
IV-236	C236	-4.47	DTCYS-CHAEK	pIC033
IV-261	P261	-4.47	VTCHN-PHGSV	pIC013
IV-301	N301	7.57	TGLGS-NVGDN	pIC018

"For each variant characterized, the table provides the name of the mutant, which is based on the native MtrA residue that follows the SGRPGSLS insertion, the identity of the amino acid that follows the insertion, the z score of the mutant from the library selection, the residues flanking the insertion site (hyphen), and the plasmid name.

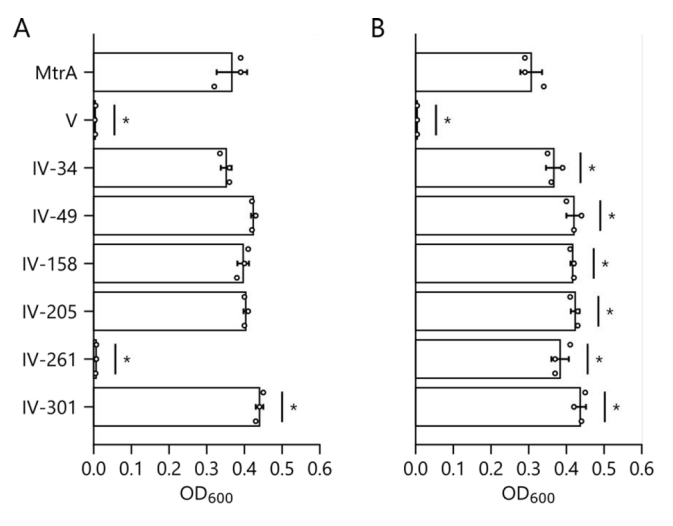


Figure 3. Complementation of $So\text{-}\Delta mtrA$ on ferric citrate by individual mutants. Cells transformed with an empty vector (V) or plasmids that express native MtrA (MtrA) and insertion variants (IV) were grown under anaerobic conditions with ferric citrate as the sole electron acceptor at 30 °C. The optical density of cultures was measured at (A) 24 and (B) 48 h. Error bars represent $\pm 1\sigma$ from three experiments. After 24 h, IV-301 grew to a significantly higher density than cells expressing native MtrA (P < 0.05; two-tailed t test). All other mutants except IV-261 grew to a significantly higher density than the vector control (P < 0.01; two-tailed t test).

mentation revealed a positive linear relationship with an r^2 of 0.93 (Figure S7). After 48 h (Figure 3B), cells expressing IV-261 complemented growth. In contrast, cells transformed with an empty vector did not present growth even after 72 h (Figure S8). All of the cultures with an OD_{600} increase also changed in color from brown to light yellow, which is consistent with the reduction of Fe(III); this color change reversed upon exposure to oxygen. To investigate if random mutations beyond the peptide insertions led to the observed growth, vectors were sequenced following growth complementation. No mutations were observed beyond the peptide insertions. These findings show that the enrichment values observed in our library experiment correlate with growth complementation of individual variants. Additionally, they show that the variants having the lowest z scores support EET, albeit with severely decreased efficiencies compared with that of native MtrA.

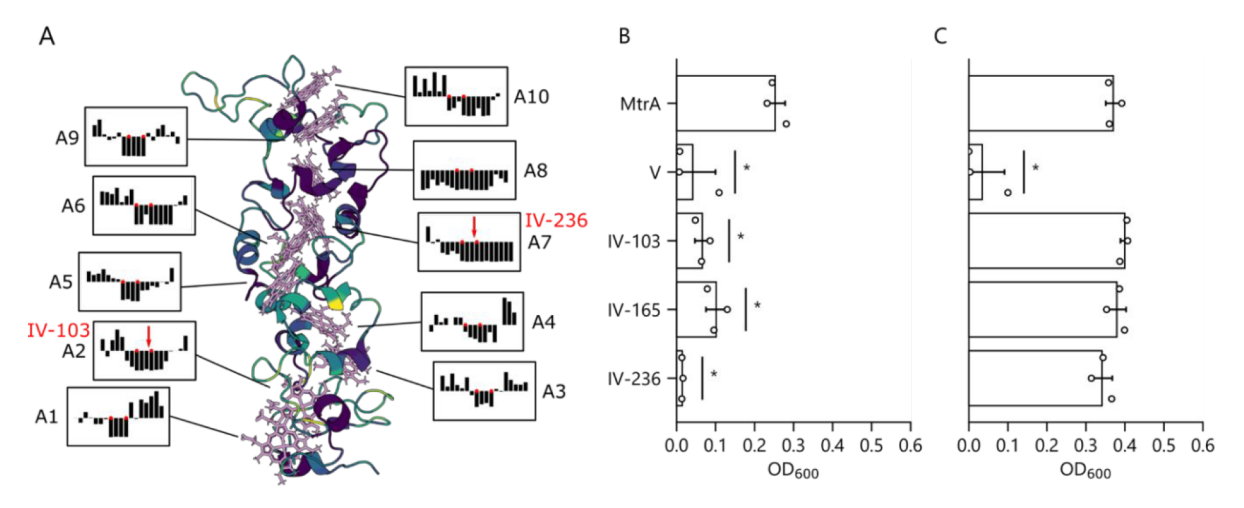


Figure 4. Effect of peptide insertion within CXXCH motifs on EET. (A) The MtrA structure is color-coded using the z scores observed in the mutational profile, and insets depicting the distribution of z scores around each of the 10 CXXCH motifs are shown. In the boxes, the red circles above the line represent the cysteines in each motif, the arrows note the insertion sites, and the black vertical bars represent the z scores proximal to these motifs. Cells transformed with an empty vector (V) or plasmids that express native MtrA (MtrA) and insertion variants (IV) were grown under anaerobic conditions with ferric citrate as the sole electron acceptor at 30 °C. The optical density of cultures was measured at (B) 24 and (C) 72 h. Error bars represent $\pm 1\sigma$ from three experiments. After 72 h, all tested IVs grew to a significantly higher density than cells expressing the vector control (P < 0.05; two-tailed t test).

Mutants with Insertions in CXXCH Motifs Support Ferric Citrate Reduction. Surprisingly, the variant depleted to the largest extent by the selection (IV-261) retained the ability to support respiration on Fe(III). For this reason, expression vectors for three additional variants (IV-103, IV-165, and IV-236) were created that present low z scores in the mutational profile (Table 1). Two of these variants, IV-103 and IV-236, were chosen because they insert a peptide within a CXXCH motif (Figure 4A) and have the potential to inhibit covalent ligation of hemes 2 and 7, respectively. All three variants were transformed into So-\DeltamtrA and evaluated for growth complementation. After 24 h, only cells expressing native MtrA showed significant growth (Figure 4B). After 72 h, cells expressing all three variants presented optical densities comparable to those of cells expressing native MtrA and significantly higher than that of the empty vector control (Figure 4C). Cultures expressing these variants all displayed a color change characteristic of Fe(III) reduction. These findings show that MtrA variants having an octapeptide inserted within a CXXCH motif retain the ability to support EET. This tolerance is surprising because structural studies suggest that hemes 2 and 7 are required for rapid electron transfer across the length of MtrA.

To determine if the octapeptide insertions decrease the amount of MtrA that accumulates as a decaheme holoprotein in cells, we measured the cytochrome c content of $So-\Delta mtrA$ cultures expressing all nine variants and native MtrA using enhanced chemiluminescence (ECL). Cells expressing MtrA presented bands consistent with the well-known cytochromes in S. oneidensis, including MtrC, MtrA, and CymA (Figure S9). In addition, two smaller cytochromes that were interpreted as representing CcmE and NapB were observed. Cells transformed with an empty vector contained all cytochromes except MtrA. In addition, the different insertion variants presented a range of MtrA levels. To account for loading variation, the intensities of MtrA bands were normalized to the band representing the smallest cytochrome, which was the most consistent cytochrome in our analysis (Figure 5A). When this normalization was performed, only a subset of the MtrA

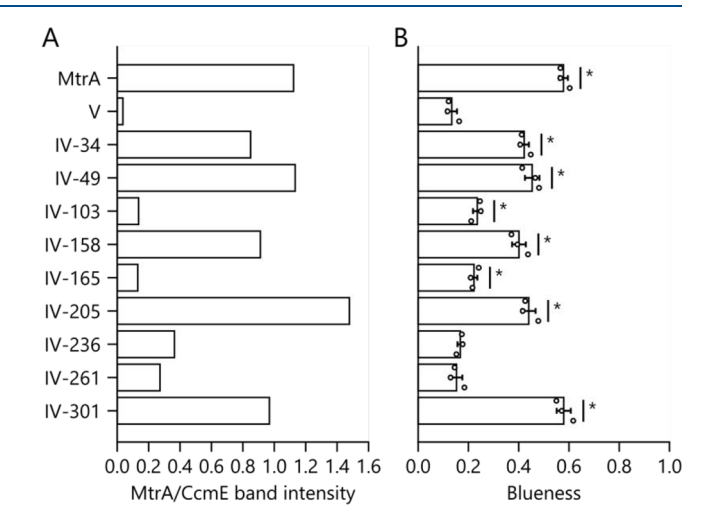


Figure 5. Effect of mutations on cytochrome maturation and EET to nanomaterials. $So\text{-}\Delta mtrA$ transformed with the empty vector (V) and plasmids expressing MtrA (MtrA) and nine different insertion variants (IV) were cultured overnight. The total protein from each sample was separated on an agarose gel and stained for cytochromes. (A) MtrA/CctA band intensity ratios for ECL samples. (B) $So\text{-}\Delta mtrA$ cells taken from the same culture as the ECL samples were incubated in M9 minimal medium containing 10 mg/L MoO₃ nanoparticles under anaerobic conditions for 15 min in a 96-well plate. The blueness of each well was quantified. Samples presenting significantly higher signal intensities compared with that of the empty vector are noted with an asterisk (P < 0.05; two-tailed t test). Error bars represent ± 1 standard deviation calculated from three experiments.

variants presented decreased levels, including two having insertions within a CXXCH motif (IV-103 and IV-236) and two with insertions outside of a heme-binding motif (IV-165 and IV-261). Surprisingly, all of these MtrA variants presented some holo-MtrA by ECL. The detection of holo-MtrA mutants having modified CXXCH motifs shows that the cytochrome ϵ maturation system can covalently attach hemes to proteins with dramatic alteration to a single CXXCH motif. In the case of the other variants that exhibited decreased holoprotein

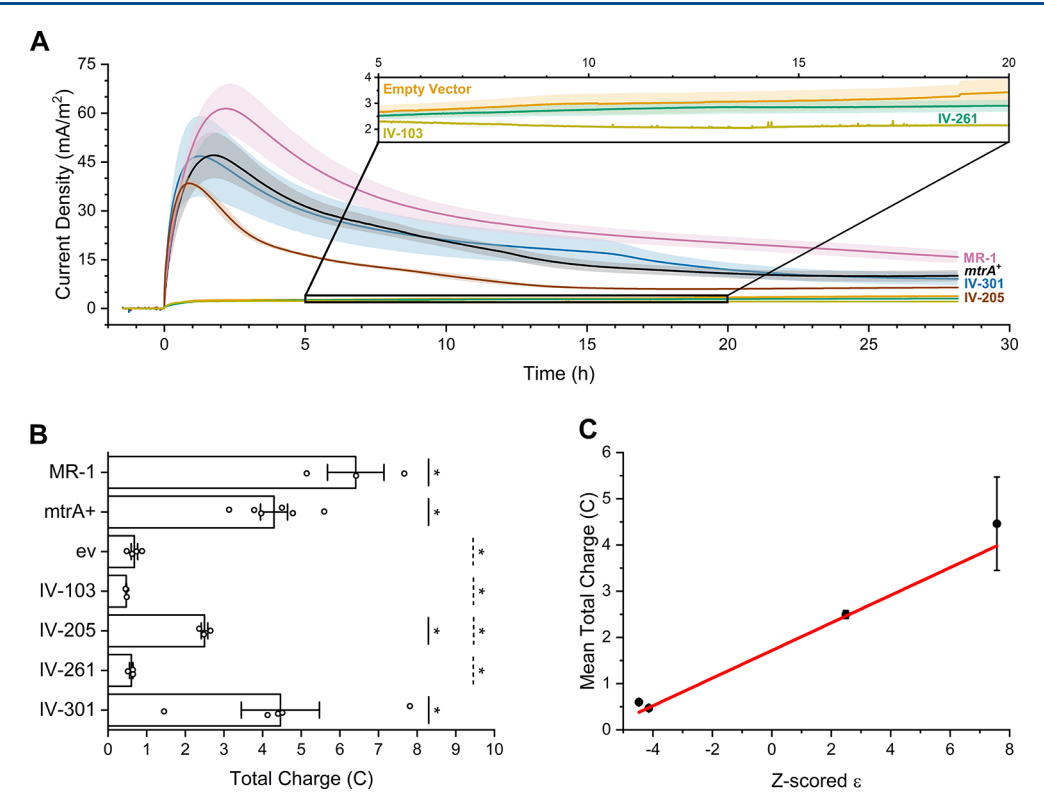


Figure 6. Effect of mutations on current in a bioelectrochemical cell. (A) Chronoamperometry of So-ΔmtrA expressing native MtrA (black), IV-261 (green), IV-301 (blue), IV-103 (yellow), IV-205 (brown), and the empty vector (orange) compared with S. oneidensis MR-1 (purple). So-ΔmtrA cells expressing IV-103 and IV-261 produce negligible current, while So-ΔmtrA cells expressing IV-205 and IV-301 approach native MtrA values. Experiments were performed using a carbon felt working electrode at 0.2 V vs Ag/AgCl (3 M KCl) with 30 mM p.L-lactate as the electron donor. Data are plotted as the mean of biological replicates for MR-1 (n = 3) and So-ΔmtrA expressing MtrA (n = 6), IV-103 (n = 3), IV-205 (n = 3), IV-261 (n = 3), IV-301 (n = 5), and So-ΔmtrA transformed with an empty vector (n = 4). Error bars represent ±1 standard error of the mean. Time is listed relative to the injection of cells into the bioelectrochemical reactor. (B) Total charge transferred to the electrode by each strain, computed by integrating the baseline-subtracted current over the period from time zero to the end of the experiment. Strains that transferred significantly more charge than the empty vector are noted with a solid line and an asterisk (P < 0.05; two-tailed P < 0.05; two-

levels as determined by ECL, this decrease could arise because the insertions occur in MtrA regions that are critical for interacting with the cytochrome *c* maturation system. Overall, these results show that peptide insertion within heme-binding motifs decreases the total holo-MtrA levels within cells, yet these mutants still mature into sufficient holo-MtrA to support cell growth that requires ferric citrate reduction.

Mutants Differentially Reduce Soluble and Insoluble Electron Acceptors. MtrA transfers electrons to the surfacedisplayed cytochrome MtrC, which in turn modulates binding¹⁴ and electron transfer to both soluble Fe(III) and insoluble extracellular materials.⁵⁸ These observations led us to hypothesize that all of our variants with decreased levels of EET to Fe(III) would also present decreased levels of EET to materials. To determine the effects of MtrA mutations on electron transfer to extracellular materials, we utilized a modified version of a nanoparticle reduction assay.⁵⁹ In this assay, we evaluated EET to MoO₃ nanoparticles (Figure S10), rather than commonly used WO3, because we found that MoO₃ particles are more sensitive for reporting on EET.⁶⁰ With this assay, the nanoparticles undergo an electrochromic shift from white to blue as electroactive microbes reduce them via EET. When we used this assay to characterize So- $\Delta mtrA$

cells expressing different insertion variants (Figure 5B and Figure S11), we found that only a subset of the variants support $\mathrm{MoO_3}$ reduction following a 15 min incubation. Cells expressing insertion variants with positive z scores showed rapid and strong reduction of the nanoparticles, with IV-301 (z=7.57) matching the reduction achieved with native MtrA. More than half of the variants with negative z scores (IV-34, IV-103, and IV-165) supported nanoparticle reduction that significantly exceeded that of the vector control, although they showed poorer reduction capabilities than variants with positive z scores.

Two variants (IV-236 and IV-261) were unable to reduce the nanoparticles beyond the negative control, even after a 96 h incubation. This finding indicates that cells expressing some insertion variants failed to reduce MoO₃ even though they were competent at reducing extracellular ferric citrate. Among the insertion variants, those that presented the greatest reduction in the nanoparticle assay had the largest abundance of holo-MtrA as judged by MtrA:CcmE ratios in the ECL analysis. In contrast, those variants with low or no signals in the nanoparticle assay exhibited faint bands at the same position. Interestingly, the MtrA:CcmE ratio of IV-236 was

greater than those of IV-103 and IV-165, both of which outperformed IV-236 in the nanoparticle assay.

To probe the effect of MtrA peptide insertion on EET that is relevant for microbial electrochemical technologies, we evaluated the ability of $So-\Delta mtrA$ strains expressing MtrA variants to reduce an electrode using chronoamperometry. We evaluated the current generated by cells expressing native MtrA and variants exhibiting a range of EET with ferric citrate and MoO₃ nanoparticles, including the most active variant (IV-301), the least active variant (IV-261), and two with intermediate z scores (IV-205 and IV-103) (Figure 6A). We hypothesized that the current observed in a bioelectrochemical system would correlate more strongly with the signal obtained with MoO₃ nanoparticles. As controls, we also evaluated the current generated by $So-\Delta mtrA$ transformed with an empty vector and wild-type S. oneidensis MR-1. With cells expressing IV-261 and IV-103 (z scores of -4.47 and -4.14, respectively), current production was indistinguishable from that of the empty vector control. In contrast, cells expressing native MtrA and IV-301 (z score = 7.57) presented similar current densities. In contrast, IV-205 (z score = 2.40) presented an intermediate current density, transferring a total charge significantly greater than that of the empty vector control yet significantly lower than that of the strain expressing native MtrA (Figure 6B). For the cells expressing insertion variants, the total charge transferred over the course of the experiment was linearly correlated with the z score observed in the library selection ($r^2 = 0.96$) on ferric citrate (Figure 6C). Like S. oneidensis MR-1, So- $\Delta mtrA$ expressing IV-301, IV-205, and MtrA showed strong initial current peaks that diminished within 5 h. These findings reveal a striking correlation between the sequence enrichments arising from the selection with a soluble electron acceptor and the current generated at an electrode. Materials like electrodes can be challenging to directly use in library selection as changes in electron flux can be confounded by changes in biofilm formation or surface interactions.⁶¹ Thus, the protein design approach used herein represents a simple way to discover MtrA mutants presenting a range of EET with metal ions and materials.

Insertion Tolerance Correlates with Heme Proximity. To evaluate the structural underpinnings for MtrA mutant activity, we mapped MtrA mutant z scores onto the S. baltica MtrA structure. Regions that led to the largest decreases in EET efficiency following peptide insertion included (i) the loops at the interface between adjacent perpendicular hemes, (ii) a loop that interacts with the MtrB pore close to the extracellular surface of the lipid bilayer, (iii) residues that are localized to the periplasm, and (iv) all 10 α -helices coordinating the 10 heme cofactors (Figure 2). The insertion tolerance (z score) is uniformly low within all 10 CXXCH heme-ligating motifs. Some of the histidine ligands outside of these motifs present similar low z scores, e.g., the distal histidines that serve as axial ligands for hemes 2, 4, 6, 8, and 9. However, the other distal histidines present a higher insertion tolerance. Unexpectedly, the interface between MtrA and MtrC shows a high level of peptide insertion tolerance. Thus, our systematic mutagenesis approach identifies diverse regions and motifs that tolerate peptide insertion without disrupting

To enable efficient ET across the outer membrane, MtrA must arrange 10 iron-containing heme prosthetic groups at optimal distances and orientations for electron transfer within a protein environment. To investigate if the peptide insertion

ı

EET.

tolerance depends upon the proximity to heme prosthetic groups, we evaluated how insertion tolerance varies with proximity to the central axis of MtrA containing the heme prosthetic groups and position along the long axis of MtrA that spans the outer membrane. Consistent with the idea that MtrA functions as a protein wire, a correlation ($r_{\rm s}=0.48$) was observed between sequence enrichment values ($\varepsilon_{\rm i}$) and radial insertion distance from the center axis of iron atoms (Figure 7A), which are coordinated by axial heme ligands. In addition,

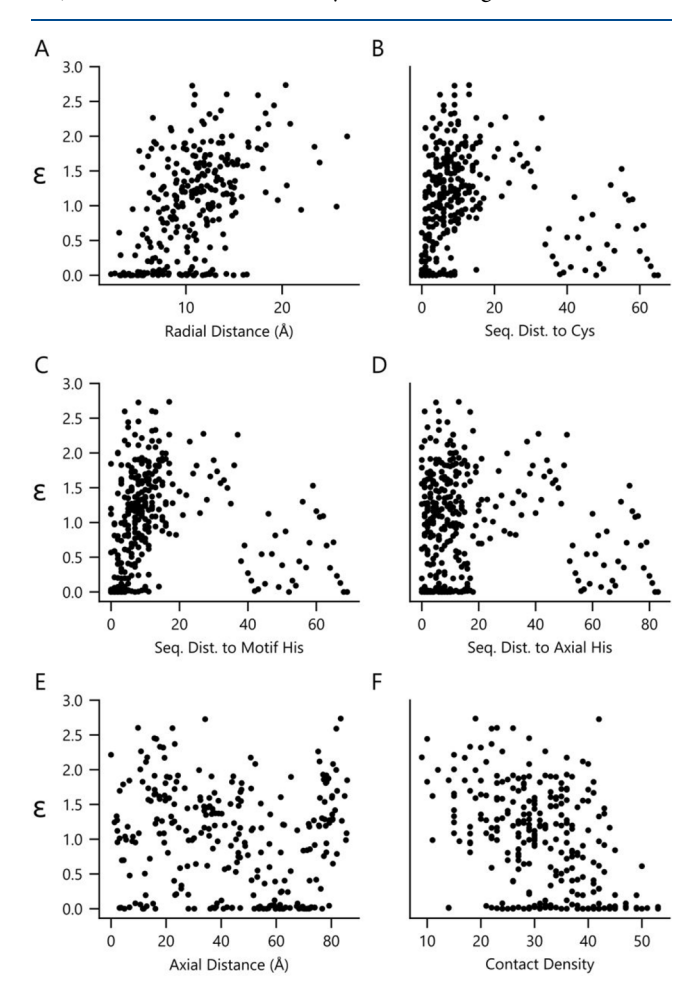


Figure 7. Comparison of the insertional tolerance and structural features in MtrA. Spearman correlations between the profile z scores and biophysical properties were evaluated, including (A) the radial distance from a central axis defined by heme iron atoms ($r_s = 0.48$; $p < 10^{-15}$), (B) the distance in primary structure from heme-binding cysteines in the CXXCH motifs ($r_s = 0.35$; $p < 10^{-10}$), (C) the distance in primary structure from the histidines within the CXXCH motifs ($r_s = 0.36$; $p < 10^{-10}$), (D) the distance in primary structure from histidine ligands outside of the CXXCH motifs ($r_s = 0.02$; p = 0.7), (E) the axial distance along the long axis of MtrA ($r_s = -0.10$; p = 0.1), and (F) \leq 14 Å intramolecular MtrA contacts ($r_s = -0.39$; $p < 10^{-10}$).

a positive correlation was observed between the insertion tolerance and the sequence distance to the nearest cysteine (r_s = 0.35) in the CXXCH motif (Figure 7B). While a similar correlation (r_s = 0.36) was observed when analyzing the relationship between insertion tolerance and the distance to the histidine ligands in the CXXCH motifs (Figure 7C), no correlation (r_s = 0.02) was observed when analyzing the relationship between insertion tolerance and sequence distance

to the axial histidine ligands that are outside of the CXXCH motifs (Figure 7D). In addition, no correlation was observed between insertion tolerance and the position along the long axis of MtrA (Figure 7E), and a weak correlation ($r_s = -0.39$) was observed between the insertion tolerance and the density of intramolecular residue-residue contacts (Figure 7F) when both short- and long-range contacts ($\leq 14 \text{ Å}$) were considered. No correlation was observed when comparing the insertion tolerance to short-range (≤8 Å) contacts (Figure S12a) and the density of interprotein residue-residue contacts between MtrA and MtrB (Figure S12b). A majority of the MtrA and MtrC residue-residue contacts presented enrichment, with a weak positive correlation observed between enrichment and the number of interprotein contacts between MtrA and MtrC (Figure S12c). No correlation was observed with B factors from the MtrA crystal structure (Figure S12d) and stiffness calculated from a coarse-grain elastic network model (Figure S12e). This latter model does not account for the residues that coordinate the heme cofactors, so it may underestimate some aspects of stiffness within the structure. Together, these analyses show that the strongest correlations are observed between the insertion tolerance and proximity to the axis of iron atoms that span the outer membrane and function as a wire, the proximity to CXXCH motifs in the primary structure, and the density of intramolecular residue-residue contacts.

DISCUSSION

Our results greatly extend our fundamental understanding of sequence-structure-EET relationships in multiheme cytochromes. Prior genetic studies revealed the functional roles that different members of the MtrCAB complex play in supporting EET to extracellular metal ions and materials. 15-17,22,62,63 However, prior to this study, only two studies examined the effect of mutations on MtrA. The first study demonstrated that the histidines within the MtrA CXXCH motifs are critical for EET,64 while the second study identified a pair of mutations in MtrA and MtrB that compensate for the loss of MtrC under anaerobic conditions.⁶⁵ Additionally, only two studies evaluated the effects of mutations on MtrC-type multiheme cytochromes, which transfer electrons to insoluble electron acceptors. These efforts revealed that the cysteines in the MtrC $\dot{\text{CX}}_{8}\text{C}$ motif form a disulfide that is critical for aerobic growth 66 and identified residues that modulate nanoparticle binding through electrostatic interactions. 14 By using a combinatorial mutagenesis approach to comprehensively evaluate the functional consequences of generating mutations at every native location in a multiheme cytochrome, we identify diverse regions across the primary structure that present a high functional tolerance to peptide insertion, such as extracellular residues proximal to the MtrA-MtrC binding interface. Additionally, we establish the motifs that are most sensitive to peptide insertion, such as the CXXCH motifs. Surprisingly, Fe(III) reduction was still observed following the insertion of an octapeptide within and proximal to the CXXCH motifs, a mutation that is expected to be more structurally disruptive than previously studied point mutations.⁶⁴ This finding suggests that individual heme-binding motifs can have their primary structure modified without completely abolishing MtrA maturation, insertion into MtrB and the outer membrane, and MtrA-mediated EET.

Our results provide insight into residue—residue contacts made by MtrA and MtrB that are critical to supporting EET. Although the mechanism of insertion of MtrA into MtrB is not

well understood, it is clear that MtrA protects MtrB from degradation, enabling expression of MtrB. 67 Indeed, the MtrB channel is narrower at the extracellular end than at the periplasmic end, leading to prior speculation that MtrB arrests MtrA in a state of stalled excretion.²⁰ The interface between MtrB and MtrA is not thought to be tight, although a solvent channel has been proposed to run between MtrB and one side of MtrA, with residues from both proteins capping this channel.²⁰ Our measurements revealed variation in the insertion tolerance proximal to MtrA residues that make contacts with MtrB. Among the diverse positions that contact MtrB, several showed a high tolerance to insertion, especially those closer to the periplasmic end of the channel. In contrast, some regions closer to the extracellular end of the channel presented marked intolerance to peptide insertion. In particular, the loop defined by MtrA residues 240-247 had a large number of MtrB contacts that exhibited a high degree of functional sensitivity to peptide insertion. These findings implicate this interacting motif as being critical to MtrAB secretion and/or stability.

Surprisingly, the interface between MtrA and MtrC did not appear to be sensitive to peptide insertion in our library selection. In fact, the peptide insertion site enriched to the greatest extent is located in an extracellular-facing loop at the MtrA-MtrC interface. The underlying mechanism by which MtrA insertion variants retain function upon peptide insertion at the MtrA-MtrC interface is not known. Prior structural studies have provided evidence that MtrA and MtrC use hydrogen bonds to position themselves closely together, with heme A10 of MtrA being only 8 Å from heme C5 of MtrC.²⁰ Additionally, genetic studies have shown that native MtrA cannot reduce ferric citrate above detectable limits in the absence of MtrC. ^{22,63} One possible explanation for the high EET efficiency observed with peptide insertion near the MtrA-MtrC binding interface is that the mutant MtrA-MtrB complexes exhibit enhanced ferric citrate reduction activity. A previous study showed that mutations in MtrA and MtrB increase the level of ferric citrate reduction in a S. oneidensis strain lacking MtrC and its homologues.⁶⁵ Whether MtrA peptide insertions allow the MtrA-MtrB complex to reduce ferric citrate will require future studies of EET in MtrC knockout strains.

The observation that some insertion variants vary in their ability to reduce soluble (ferric citrate) and insoluble (nanomaterials and electrode) electron acceptors suggests that some insertion variants may not require MtrC to respire. In a prior study, a mutated MtrA-MtrB complex could reduce soluble extracellular acceptors in the absence of MtrC, such as 9,10-anthraquinone-2,7-disulfonic acid (AQDS) and ferric citrate.65 However, the ability of these mutants to reduce insoluble extracellular acceptors like birnessite and pahokee peat humic acids is diminished.⁶⁵ This observation highlights the role that MtrC plays in facilitating EET to larger terminal electron acceptors. Taken together with our results, this finding suggests that MtrA insertion variants that retain the ability to reduce ferric citrate but fail to reduce insoluble extracellular electron acceptors may be operating in an MtrC-independent manner. This trend is expected to occur when peptide insertion disrupts the interaction between heme A10 in MtrA and heme C5 in MtrC, which could arise from steric clashes caused by peptide insertion or conformational changes in MtrA induced by peptide insertions. ET between these hemes is thought to be the slowest within the MtrCAB

complex, and a subtle structural change in one of these prosthetic groups could disrupt ET from MtrA to MtrC, cutting off MtrC from the rest of the pathway. To establish whether MtrA functions in an MtrC-independent manner, additional biophysical studies will be needed to establish how peptide insertions affect the affinity of MtrA for MtrC, as well as the distance and orientation between heme A10 in MtrA and heme C5 in MtrC.

The N-terminus of MtrA, which is unresolved in the MtrA crystal structure, 20 exhibited a low tolerance to peptide insertion. This region does not ligate a heme, so this trend is not thought to arise from the disruption of MtrA electron transfer. This trend could arise through different mechanisms. First, the initial 34 residues in MtrA comprise the signal peptide sequence responsible for translocation across the inner membrane, which is cleaved during cytochrome maturation and trafficking.⁵⁸ Disruption of this motif could impede interaction with the Sec translocase, alter processing and maturation, and decrease the amount of MtrA that enters the periplasm.⁶⁸ Second, peptide insertion near the N-terminus could decrease the level of MtrA expression due to the proximity to the RBS that regulates translation initiation. A thermodynamic model has revealed that mutations proximal to an RBS can generate local RNA structures that compete with ribosome binding.⁶⁹ Third, peptide insertion could disrupt the region of MtrA that mediates binding to periplasmic electron carriers. Genetic and structural studies have implicated several periplasmic and inner membrane-bound oxidoreductases in reducing MtrA, including CymA, CctA, and FccA. 22,70,71 Given that CctA is knocked out in the strain we utilized for our selection assays (JG665), the sensitivity of MtrA to insertions at the N-terminus suggests this region mediates contact with CymA or FccA.²² In the future, it will be interesting to select MtrA mutant libraries in strains that contain different periplasmic electron carriers and to compare the results to determine if residues in the N-terminal region of MtrA present a similar functional sensitivity to peptide insertion. Additionally, it will be interesting to investigate how peptide insertions affect interactions with the cyt c maturation (ccm) machinery, which relays heme substrates for the ligation reaction and catalyzes the formation of the thioester bonds with the CXXCH motifs in MtrA.⁵⁹ Prior studies have shown that the ccm machinery can be modified to improve the bioelectronic performance of E. coli expressing the Mtr system.⁵⁹ This observation suggests that modification to the ccm system could affect the EET mediated by the active mutants selected in this

Our results suggest that the underlying mechanism by which peptide insertion disrupts EET may vary from mutant to mutant. For example, ECL measurements of holo-MtrA suggest that the decreased level of EET to MoO₃ nanoparticles may arise because the total amount of holoprotein that accumulates in the membrane is diminished. This appears to occur with IV-165 and IV-261, which present both decreased levels of EET to MoO3 nanoparticles and decreased MtrA:CcmE ratios. However, the MtrA:CcmE ratios of other insertion variants such as IV-236 were higher than that of IV-165, yet it presented weaker EET in the nanoparticle assay. This finding suggests that peptide insertion in IV-236 has little effect on holo-MtrA levels but instead disrupts EET by disrupting the distances and orientations of a heme prosthetic group or by altering the binding affinity for partner oxidoreductases like MtrC and periplasmic carrier partners.

The library approach herein represents an excellent starting point for further probing sequence-structure-EET relationships in multiheme cytochromes. Similar libraries can be generated with other members of the MtrCAB complex to better understand critical residues for their molecular interactions. Additionally, larger insertions can be introduced into these proteins to better understand how they can be engineered for bioelectronics applications.⁷² In future studies, it will be interesting to investigate whether MtrA variants can be created that report on chemical information in the environment by regulating EET post-translationally. A recent study showed that EET can be regulated through ligand binding to a cytosolic ferredoxin protein electron carrier. 73,74 Allosteric protein switches that control EET on the extracellular face of cells would have distinct advantages over cytosolic ferredoxin protein switches because they would be regulated by analyte concentrations in the extracellular environment, which can be distinct from the concentrations that enter the cell.

ASSOCIATED CONTENT

Supporting Information

The Supporting Information is available free of charge at https://pubs.acs.org/doi/10.1021/acs.biochem.2c00148.

Naive library sequence abundances (Figure S1), library frequency distributions (Figure S2), nonselected library sequence abundances (Figure S3), comparison of nonselected and naive sequence frequencies (Figure S4), selected library sequence abundances (Figure S5), mutant enrichment values (Figure S6), growth complementation after 1 day (Figure S7), growth complementation after 3 days (Figure S8), cytochrome maturation (Figure S9), nanoparticle assay comparison (Figure S10), blueness assay images (Figure S11), structural correlations with insertion tolerance (Figure S12), MtrA sequence alignment (Figure S13), and assay vectors (Table S1) (PDF)

Insertion frequency data (Table S2) (XLSX)

Accession Codes

MtrA, Q8EG35; MtrB, Q8CVD4; MtrC, Q8EG34.

AUTHOR INFORMATION

Corresponding Author

Jonathan J. Silberg — Department of BioSciences, Rice University, Houston, Texas 77005, United States; Department of Bioengineering, Rice University, Houston, Texas 77005, United States; Department of Chemical and Biomolecular Engineering, Rice University, Houston, Texas 77005, United States; orcid.org/0000-0001-5612-0667; Phone: 713-348-3849; Email: joff@rice.edu

Authors

Ian J. Campbell – Department of BioSciences, Rice University, Houston, Texas 77005, United States; ⊚ orcid.org/0000-0003-3944-1260

Joshua T. Atkinson – Department of Physics and Astronomy, University of Southern California, Los Angeles, California 90089, United States; orcid.org/0000-0001-9293-4123

Matthew D. Carpenter – Department of BioSciences, Rice University, Houston, Texas 77005, United States

Dru Myerscough – Department of BioSciences, Rice University, Houston, Texas 77005, United States

Lin Su − Department of Chemistry, University of Cambridge, Cambridge CB2 1EW, United Kingdom; © orcid.org/0000-0001-8784-3120

Caroline M. Ajo-Franklin – Department of BioSciences, Rice University, Houston, Texas 77005, United States; Department of Bioengineering, Rice University, Houston, Texas 77005, United States

Complete contact information is available at: https://pubs.acs.org/10.1021/acs.biochem.2c00148

Author Contributions

I.J.C., J.T.A., and J.J.S. conceptualized the project. I.J.C. and J.T.A. constructed the library. I.J.C. performed selections. I.J.C. and M.D.C. performed ECL analysis. I.J.C., L.S., and M.D.C. performed nanoparticle assays. M.D.C. conducted the electrochemistry measurements. I.J.C. and D.M. conducted structural analysis. I.J.C. and J.J.S. drafted the article, and all authors contributed to the text.

Funding

Funding was provided by Office of Naval Research Grant N00014-20-1-2274 (to C.M.A.-F. and J.J.S.); Office of Science, Office of Basic Energy Sciences of the U.S. Department of Energy Grant DE-SC0014462 (to J.J.S.); Cancer Prevention and Research Institute of Texas Grant RR190063 (to C.M.A.-F.); and National Science Foundation (NSF) Grant 1843556 (to J.J.S.). M.D.C. is supported by NSF National Research Traineeship in Bioelectronics Grant 1828869, and J.T.A. is supported by NSF Postdoctoral Research Fellowship in Biology Grant No. 2010604. Modeling was supported by Rice University's Center for Research Computing and the Big-Data Private-Cloud Research Cyberinfrastructure NSF MRIaward (1338099). S. oneidensis JG665 (So-ΔmtrA) was a kind gift from Dr. Jeff Gralnick.

Notes

The authors declare no competing financial interest.

■ REFERENCES

- (1) Baker, I. R.; Conley, B. E.; Gralnick, J. A.; Girguis, P. R. Evidence for Horizontal and Vertical Transmission of Mtr-Mediated Extracellular Electron Transfer among the Bacteria. *mBio* **2022**, *13* (1), e0290421.
- (2) Shi, L.; Dong, H.; Reguera, G.; Beyenal, H.; Lu, A.; Liu, J.; Yu, H.-Q.; Fredrickson, J. K. Extracellular Electron Transfer Mechanisms between Microorganisms and Minerals. *Nat. Rev. Microbiol* **2016**, *14* (10), 651–662.
- (3) Jiang, X.; Burger, B.; Gajdos, F.; Bortolotti, C.; Futera, Z.; Breuer, M.; Blumberger, J. Kinetics of Trifurcated Electron Flow in the Decaheme Bacterial Proteins MtrC and MtrF. *Proc. Natl. Acad. Sci. U. S. A.* **2019**, *116* (9), 3425–3430.
- (4) Jiang, X.; van Wonderen, J. H.; Butt, J. N.; Edwards, M. J.; Clarke, T. A.; Blumberger, J. Which Multi-Heme Protein Complex Transfers Electrons More Efficiently? Comparing MtrCAB from Shewanella with OmcS from Geobacter. *J. Phys. Chem. Lett.* **2020**, *11* (21), 9421–9425.
- (5) Jiang, X.; Futera, Z.; Ali, M. E.; Gajdos, F.; von Rudorff, G. F.; Carof, A.; Breuer, M.; Blumberger, J. Cysteine Linkages Accelerate Electron Flow through Tetra-Heme Protein STC. *J. Am. Chem. Soc.* **2017**, *139* (48), 17237–17240.
- (6) van Wonderen, J. H.; Adamczyk, K.; Wu, X.; Jiang, X.; Piper, S. E. H.; Hall, C. R.; Edwards, M. J.; Clarke, T. A.; Zhang, H.; Jeuken, L. J. C.; Sazanovich, I. V.; Towrie, M.; Blumberger, J.; Meech, S. R.; Butt, J. N. Nanosecond Heme-to-Heme Electron Transfer Rates in a Multiheme Cytochrome Nanowire Reported by a Spectrally Unique

- His/Met-Ligated Heme. Proc. Natl. Acad. Sci. U. S. A. 2021, 118 (39), e2107939118.
- (7) Jiang, J.; Kappler, A. Kinetics of Microbial and Chemical Reduction of Humic Substances: Implications for Electron Shuttling. *Environ. Sci. Technol.* **2008**, 42 (10), 3563–3569.
- (8) Yang, Z.; Sun, T.; Subdiaga, E.; Obst, M.; Haderlein, S. B.; Maisch, M.; Kretzschmar, R.; Angenent, L. T.; Kappler, A. Aggregation-Dependent Electron Transfer via Redox-Active Biochar Particles Stimulate Microbial Ferrihydrite Reduction. *Sci. Total Environ.* 2020, 703, 135515.
- (9) Bai, Y.; Mellage, A.; Cirpka, O. A.; Sun, T.; Angenent, L. T.; Haderlein, S. B.; Kappler, A. AQDS and Redox-Active NOM Enables Microbial Fe(III)-Mineral Reduction at Cm-Scales. *Environ. Sci. Technol.* **2020**, *54* (7), 4131–4139.
- (10) Myers, C. R.; Nealson, K. H. Bacterial Manganese Reduction and Growth with Manganese Oxide as the Sole Electron Acceptor. *Science* **1988**, 240 (4857), 1319–1321.
- (11) Beliaev, A. S.; Saffarini, D. A. Shewanella Putrefaciens MtrB Encodes an Outer Membrane Protein Required for Fe(III) and Mn(IV) Reduction. *J. Bacteriol.* **1998**, *180* (23), 6292–6297.
- (12) Lower, B. H.; Shi, L.; Yongsunthon, R.; Droubay, T. C.; McCready, D. E.; Lower, S. K. Specific Bonds between an Iron Oxide Surface and Outer Membrane Cytochromes MtrC and OmcA from Shewanella Oneidensis MR-1. *J. Bacteriol.* **2007**, *189* (13), 4944–4952.
- (13) Xiong, Y.; Shi, L.; Chen, B.; Mayer, M. U.; Lower, B. H.; Londer, Y.; Bose, S.; Hochella, M. F.; Fredrickson, J. K.; Squier, T. C. High-Affinity Binding and Direct Electron Transfer to Solid Metals by the Shewanella Oneidensis MR-1 Outer Membrane c-Type Cytochrome OmcA. J. Am. Chem. Soc. 2006, 128 (43), 13978–13979.
- (14) Fukushima, T.; Gupta, S.; Rad, B.; Cornejo, J. A.; Petzold, C. J.; Chan, L. J. G.; Mizrahi, R. A.; Ralston, C. Y.; Ajo-Franklin, C. M. The Molecular Basis for Binding of an Electron Transfer Protein to a Metal Oxide Surface. *J. Am. Chem. Soc.* **2017**, *139* (36), 12647–12654.
- (15) Coursolle, D.; Baron, D. B.; Bond, D. R.; Gralnick, J. A. The Mtr Respiratory Pathway Is Essential for Reducing Flavins and Electrodes in Shewanella Oneidensis. *J. Bacteriol.* **2010**, 192 (2), 467–474.
- (16) Dundas, C. M.; Graham, A. J.; Romanovicz, D. K.; Keitz, B. K. Extracellular Electron Transfer by Shewanella Oneidensis Controls Palladium Nanoparticle Phenotype. *ACS Synth. Biol.* **2018**, *7* (12), 2726–2736.
- (17) Marshall, M. J.; Beliaev, A. S.; Dohnalkova, A. C.; Kennedy, D. W.; Shi, L.; Wang, Z.; Boyanov, M. I.; Lai, B.; Kemner, K. M.; McLean, J. S.; Reed, S. B.; Culley, D. E.; Bailey, V. L.; Simonson, C. J.; Saffarini, D. A.; Romine, M. F.; Zachara, J. M.; Fredrickson, J. K. C-Type Cytochrome-Dependent Formation of U(IV) Nanoparticles by Shewanella Oneidensis. *PLoS Biol.* **2006**, *4* (9), e268.
- (18) Hau, H. H.; Gralnick, J. A. Ecology and Biotechnology of the Genus Shewanella. *Annu. Rev. Microbiol.* **2007**, *61*, 237–258.
- (19) Breuer, M.; Rosso, K. M.; Blumberger, J.; Butt, J. N. Multi-Haem Cytochromes in Shewanella Oneidensis MR-1: Structures, Functions and Opportunities. *J. R Soc. Interface* **2015**, *12* (102), 20141117.
- (20) Edwards, M. J.; White, G. F.; Butt, J. N.; Richardson, D. J.; Clarke, T. A. The Crystal Structure of a Biological Insulated Transmembrane Molecular Wire. *Cell* **2020**, *181* (3), 665–673.e10.
- (21) Schwalb, C.; Chapman, S. K.; Reid, G. A. The Tetraheme Cytochrome CymA Is Required for Anaerobic Respiration with Dimethyl Sulfoxide and Nitrite in Shewanella Oneidensis. *Biochemistry* **2003**, *42* (31), 9491–9497.
- (22) Coursolle, D.; Gralnick, J. A. Modularity of the Mtr Respiratory Pathway of Shewanella Oneidensis Strain MR-1. *Mol. Microbiol.* **2010**, 77 (4), 995–1008.
- (23) Alves, A. S.; Costa, N. L.; Tien, M.; Louro, R. O.; Paquete, C. M. Modulation of the Reactivity of Multiheme Cytochromes by Site-Directed Mutagenesis: Moving towards the Optimization of Microbial

- Electrochemical Technologies. J. Biol. Inorg. Chem. 2017, 22 (1), 87–97.
- (24) Edwards, M. J.; White, G. F.; Lockwood, C. W.; Lawes, M. C.; Martel, A.; Harris, G.; Scott, D. J.; Richardson, D. J.; Butt, J. N.; Clarke, T. A. Structural Modeling of an Outer Membrane Electron Conduit from a Metal-Reducing Bacterium Suggests Electron Transfer via Periplasmic Redox Partners. *J. Biol. Chem.* **2018**, 293 (21), 8103–8112.
- (25) Dougherty, M. J.; Arnold, F. H. Directed Evolution: New Parts and Optimized Function. *Curr. Opin Biotechnol* **2009**, 20 (4), 486–491.
- (26) Romero, P. A.; Arnold, F. H. Exploring Protein Fitness Landscapes by Directed Evolution. *Nat. Rev. Mol. Cell Biol.* **2009**, *10* (12), 866–876.
- (27) Mehlhoff, J. D.; Ostermeier, M. Biological Fitness Landscapes by Deep Mutational Scanning. *Methods Enzymol* **2020**, *643*, 203–224.
- (28) Coyote-Maestas, W.; Nedrud, D.; Okorafor, S.; He, Y.; Schmidt, D. Targeted Insertional Mutagenesis Libraries for Deep Domain Insertion Profiling. *Nucleic Acids Res.* **2020**, *48* (2), e11.
- (29) Higgins, S. A.; Savage, D. F. Protein Science by DNA Sequencing: How Advances in Molecular Biology Are Accelerating Biochemistry. *Biochemistry* **2018**, *57* (1), 38–46.
- (30) Warren, T. D.; Patel, K.; Rivera, J. L.; Eshleman, J. R.; Ostermeier, M. Comprehensive Mutagenesis on Yeast Cytosine Deaminase Yields Improvements in 5-fluorocytosine Toxicity in HT1080 Cells. *AIChE J.* **2020**, *66* (3), e16688 DOI: 10.1002/aic.16688.
- (31) Lind, P. A.; Arvidsson, L.; Berg, O. G.; Andersson, D. I. Variation in Mutational Robustness between Different Proteins and the Predictability of Fitness Effects. *Mol. Biol. Evol.* **2017**, 34 (2), 408–418.
- (32) Mehlhoff, J. D.; Stearns, F. W.; Rohm, D.; Wang, B.; Tsou, E.-Y.; Dutta, N.; Hsiao, M.-H.; Gonzalez, C. E.; Rubin, A. F.; Ostermeier, M. Collateral Fitness Effects of Mutations. *Proc. Natl. Acad. Sci. U. S. A.* **2020**, *117* (21), 11597–11607.
- (33) Melamed, D.; Young, D. L.; Gamble, C. E.; Miller, C. R.; Fields, S. Deep Mutational Scanning of an RRM Domain of the Saccharomyces Cerevisiae Poly(A)-Binding Protein. RNA 2013, 19 (11), 1537–1551.
- (34) Engler, C.; Kandzia, R.; Marillonnet, S. A One Pot, One Step, Precision Cloning Method with High Throughput Capability. *PLoS One* **2008**, 3 (11), e3647.
- (35) Frey, J.; Bagdasarian, M. M.; Bagdasarian, M. Replication and Copy Number Control of the Broad-Host-Range Plasmid RSF1010. *Gene* **1992**, *113* (1), 101–106.
- (36) Bosley, A. D.; Ostermeier, M. Mathematical Expressions Useful in the Construction, Description and Evaluation of Protein Libraries. *Biomol Eng.* **2005**, *22* (1–3), 57–61.
- (37) Baron, D.; LaBelle, E.; Coursolle, D.; Gralnick, J. A.; Bond, D. R. Electrochemical Measurement of Electron Transfer Kinetics by Shewanella Oneidensis MR-1. *J. Biol. Chem.* **2009**, 284 (42), 28865–28873.
- (38) Nadler, D. C.; Morgan, S.-A.; Flamholz, A.; Kortright, K. E.; Savage, D. F. Rapid Construction of Metabolite Biosensors Using Domain-Insertion Profiling. *Nat. Commun.* **2016**, *7*, 12266.
- (39) Harris, C. R.; Millman, K. J.; van der Walt, S. J.; Gommers, R.; Virtanen, P.; Cournapeau, D.; Wieser, E.; Taylor, J.; Berg, S.; Smith, N. J.; Kern, R.; Picus, M.; Hoyer, S.; van Kerkwijk, M. H.; Brett, M.; Haldane, A.; Del Río, J. F.; Wiebe, M.; Peterson, P.; Gérard-Marchant, P.; Sheppard, K.; Reddy, T.; Weckesser, W.; Abbasi, H.; Gohlke, C.; Oliphant, T. E. Array Programming with NumPy. *Nature* **2020**, 585 (7825), 357–362.
- (40) Angelani, C. R.; Carabias, P.; Cruz, K. M.; Delfino, J. M.; de Sautu, M.; Espelt, M. V.; Ferreira-Gomes, M. S.; Gómez, G. E.; Mangialavori, I. C.; Manzi, M.; Pignataro, M. F.; Saffioti, N. A.; Salvatierra Fréchou, D. M.; Santos, J.; Schwarzbaum, P. J. A Metabolic Control Analysis Approach to Introduce the Study of Systems in Biochemistry: The Glycolytic Pathway in the Red Blood Cell. *Biochem Mol. Biol. Educ* 2018, 46 (5), 502–515.

- (41) Stein, A.; Kortemme, T. Improvements to Robotics-Inspired Conformational Sampling in Rosetta. *PLoS One* **2013**, *8* (5), e63090.
- (42) Kozma, D.; Simon, I.; Tusnády, G. E. CMWeb: An Interactive on-Line Tool for Analysing Residue-Residue Contacts and Contact Prediction Methods. *Nucleic Acids Res.* **2012**, *40* (W1), W329–W333.
- (43) Nagarajan, R.; Archana, A.; Thangakani, A. M.; Jemimah, S.; Velmurugan, D.; Gromiha, M. M. PDBparam: Online Resource for Computing Structural Parameters of Proteins. *Bioinf. Biol. Insights* **2016**, *10*, 73–80.
- (44) Golinski, A. W.; Holec, P. V.; Mischler, K. M.; Hackel, B. J. Biophysical Characterization Platform Informs Protein Scaffold Evolvability. ACS Comb. Sci. 2019, 21 (4), 323–335.
- (45) Hamelryck, T.; Manderick, B. PDB File Parser and Structure Class Implemented in Python. *Bioinformatics* **2003**, *19* (17), 2308–2310
- (46) Cock, P. J. A.; Antao, T.; Chang, J. T.; Chapman, B. A.; Cox, C. J.; Dalke, A.; Friedberg, I.; Hamelryck, T.; Kauff, F.; Wilczynski, B.; de Hoon, M. J. L. Biopython: Freely Available Python Tools for Computational Molecular Biology and Bioinformatics. *Bioinformatics* **2009**, 25 (11), 1422–1423.
- (47) Bakan, A.; Meireles, L. M.; Bahar, I. ProDy: Protein Dynamics Inferred from Theory and Experiments. *Bioinformatics* **2011**, *27* (11), 1575–1577.
- (48) Zhang, S.; Krieger, J. M.; Zhang, Y.; Kaya, C.; Kaynak, B.; Mikulska-Ruminska, K.; Doruker, P.; Li, H.; Bahar, I. ProDy 2.0: Increased Scale and Scope after 10 Years of Protein Dynamics Modelling with Python. *Bioinformatics* **2021**, btab187.
- (49) Coyote-Maestas, W.; Nedrud, D.; Suma, A.; He, Y.; Matreyek, K. A.; Fowler, D. M.; Carnevale, V.; Myers, C. L.; Schmidt, D. The Biophysical Basis of Protein Domain Compatibility. *bioRxiv* **2020**, DOI: 10.1101/2020.12.09.418442.
- (50) Reback, J.; McKinney, W.; Jbrockmendel; Bossche, J. V. D.; Augspurger, T.; Cloud, P.; Gfyoung; Sinhrks; Klein, A.; Roeschke, M.; Hawkins, S.; Tratner, J.; She, C.; Ayd, W.; Petersen, T.; Garcia, M.; Schendel, J.; Hayden, A.; Jancauskas, V.; Battiston, P.; Seabold, S.; Vetinari, H.; Hoyer, S.; Overmeire, W.; Dong, K.; Whelan, C.; Mehyar, M. *Pandas-Dev/Pandas: Pandas 1.0.3*; Zenodo, 2020.
- (51) Maier, T. M.; Myers, J. M.; Myers, C. R. Identification of the Gene Encoding the Sole Physiological Fumarate Reductase in Shewanella Oneidensis MR-1. *J. Basic Microbiol* **2003**, *43* (4), 312–327.
- (52) Macaluso, A.; Mettus, A. M. Efficient Transformation of Bacillus Thuringiensis Requires Nonmethylated Plasmid DNA. *J. Bacteriol.* **1991**, *173* (3), 1353–1356.
- (53) Corts, A. D.; Thomason, L. C.; Gill, R. T.; Gralnick, J. A. A New Recombineering System for Precise Genome-Editing in Shewanella Oneidensis Strain MR-1 Using Single-Stranded Oligonucleotides. *Sci. Rep* **2019**, *9* (1), 39.
- (54) Jones, A. M.; Mehta, M. M.; Thomas, E. E.; Atkinson, J. T.; Segall-Shapiro, T. H.; Liu, S.; Silberg, J. J. The Structure of a Thermophilic Kinase Shapes Fitness upon Random Circular Permutation. *ACS Synth. Biol.* **2016**, *5* (5), 415–425.
- (55) Atkinson, J. T.; Jones, A. M.; Zhou, Q.; Silberg, J. J. Circular Permutation Profiling by Deep Sequencing Libraries Created Using Transposon Mutagenesis. *Nucleic Acids Res.* **2018**, *46* (13), e76.
- (56) Zeng, Y.; Jones, A. M.; Thomas, E. E.; Nassif, B.; Silberg, J. J.; Segatori, L. A Split Transcriptional Repressor That Links Protein Solubility to an Orthogonal Genetic Circuit. *ACS Synth. Biol.* **2018**, 7 (9), 2126–2138.
- (57) Atkinson, J. T.; Jones, A. M.; Nanda, V.; Silberg, J. J. Protein Tolerance to Random Circular Permutation Correlates with Thermostability and Local Energetics of Residue-Residue Contacts. *Protein Eng. Des Sel* **2019**, 32 (11), 489–501.
- (\$8) Pitts, K. E.; Dobbin, P. S.; Reyes-Ramirez, F.; Thomson, A. J.; Richardson, D. J.; Seward, H. E. Characterization of the Shewanella Oneidensis MR-1 Decaheme Cytochrome MtrA: Expression in Escherichia Coli Confers the Ability to Reduce Soluble Fe(III) Chelates. J. Biol. Chem. 2003, 278 (30), 27758–27765.

- (59) Su, L.; Fukushima, T.; Prior, A.; Baruch, M.; Zajdel, T. J.; Ajo-Franklin, C. M. Modifying Cytochrome c Maturation Can Increase the Bioelectronic Performance of Engineered Escherichia Coli. *ACS Synth. Biol.* **2020**, *9* (1), 115–124.
- (60) Yuan, S.-J.; Li, W.-W.; Cheng, Y.-Y.; He, H.; Chen, J.-J.; Tong, Z.-H.; Lin, Z.-Q.; Zhang, F.; Sheng, G.-P.; Yu, H.-Q. A Plate-Based Electrochromic Approach for the High-Throughput Detection of Electrochemically Active Bacteria. *Nat. Protoc* **2014**, *9* (1), 112–119.
- (61) Kees, E. D.; Levar, C. E.; Miller, S. P.; Bond, D. R.; Gralnick, J. A.; Dean, A. M. Survival of the First Rather than the Fittest in a Shewanella Electrode Biofilm. *Commun. Biol.* **2021**, *4* (1), 536.
- (62) Han, R.; Liu, T.; Li, F.; Li, X.; Chen, D.; Wu, Y. Dependence of Secondary Mineral Formation on Fe(II) Production from Ferrihydrite Reduction by Shewanella Oneidensis MR-1. ACS Earth Space Chem. **2018**, 2 (4), 399–409.
- (63) Bücking, C.; Popp, F.; Kerzenmacher, S.; Gescher, J. Involvement and Specificity of Shewanella Oneidensis Outer Membrane Cytochromes in the Reduction of Soluble and Solid-Phase Terminal Electron Acceptors. FEMS Microbiol Lett. 2010, 306 (2), 144–151.
- (64) Reyes, C.; Qian, F.; Zhang, A.; Bondarev, S.; Welch, A.; Thelen, M. P.; Saltikov, C. W. Characterization of Axial and Proximal Histidine Mutations of the Decaheme Cytochrome MtrA from Shewanella Sp. Strain ANA-3 and Implications for the Electron Transport System. J. Bacteriol. 2012, 194 (21), 5840–5847.
- (65) Bücking, C.; Piepenbrock, A.; Kappler, A.; Gescher, J. Outer-Membrane Cytochrome-Independent Reduction of Extracellular Electron Acceptors in Shewanella Oneidensis. *Microbiology* **2012**, 158 (Part 8), 2144–2157.
- (66) Edwards, M. J.; White, G. F.; Norman, M.; Tome-Fernandez, A.; Ainsworth, E.; Shi, L.; Fredrickson, J. K.; Zachara, J. M.; Butt, J. N.; Richardson, D. J.; Clarke, T. A. Redox Linked Flavin Sites in Extracellular Decaheme Proteins Involved in Microbe-Mineral Electron Transfer. Sci. Rep 2015, 5, 11677.
- (67) Schicklberger, M.; Bücking, C.; Schuetz, B.; Heide, H.; Gescher, J. Involvement of the Shewanella Oneidensis Decaheme Cytochrome MtrA in the Periplasmic Stability of the Beta-Barrel Protein MtrB. *Appl. Environ. Microbiol.* **2011**, 77 (4), 1520–1523.
- (68) Rollauer, S. E.; Sooreshjani, M. A.; Noinaj, N.; Buchanan, S. K. Outer Membrane Protein Biogenesis in Gram-Negative Bacteria. *Philos. Trans R Soc. Lond B Biol. Sci.* **2015**, 370 (1679), 20150023.
- (69) Salis, H. M.; Mirsky, E. A.; Voigt, C. A. Automated Design of Synthetic Ribosome Binding Sites to Control Protein Expression. *Nat. Biotechnol.* **2009**, 27 (10), 946–950.
- (70) Fonseca, B. M.; Paquete, C. M.; Neto, S. E.; Pacheco, I.; Soares, C. M.; Louro, R. O. Mind the Gap: Cytochrome Interactions Reveal Electron Pathways across the Periplasm of Shewanella Oneidensis MR-1. *Biochem. J.* **2013**, 449 (1), 101–108.
- (71) Schuetz, B.; Schicklberger, M.; Kuermann, J.; Spormann, A. M.; Gescher, J. Periplasmic Electron Transfer via the C-Type Cytochromes MtrA and FccA of Shewanella Oneidensis MR-1. *Appl. Environ. Microbiol.* **2009**, 75 (24), 7789–7796.
- (72) Atkinson, J. T.; Su, L.; Zhang, X.; Bennett, G. N.; Silberg, J. J.; Ajo-Franklin, C. M. Real-Time Environmental Monitoring of Contaminants Using Living Electronic Sensors. *bioRxiv* **2021**, DOI: 10.1101/2021.06.04.447163.
- (73) Atkinson, J. T.; Campbell, I. J.; Thomas, E. E.; Bonitatibus, S. C.; Elliott, S. J.; Bennett, G. N.; Silberg, J. J. Metalloprotein Switches That Display Chemical-Dependent Electron Transfer in Cells. *Nat. Chem. Biol.* **2019**, *15* (2), 189–195.
- (74) Wu, B.; Atkinson, J. T.; Kahanda, D.; Bennett, G. N.; Silberg, J. J. Combinatorial Design of Chemical-dependent Protein Switches for Controlling Intracellular Electron Transfer. *AIChE J.* **2020**, *66* (3), e16796.